

# Spin-controlled Mott-Hubbard bands in $\text{LaMnO}_3$ probed by optical ellipsometry

N.N. Kovaleva,<sup>1,\*</sup> A.V. Boris,<sup>1</sup> C. Bernhard,<sup>1</sup> A. Kulakov,<sup>1,\*</sup>  
A. Pimenov,<sup>2</sup> A.M. Balbashov,<sup>3</sup> G. Khaliullin,<sup>1</sup> and B. Keimer<sup>1</sup>

<sup>1</sup>*Max-Planck-Institut für Festkörperforschung, Heisenbergstrasse 1, D-70569 Stuttgart, Germany*

<sup>2</sup>*Experimentalphysik V, Institut für Physik, Universität Augsburg, 86135 Augsburg, Germany*

<sup>3</sup>*Moscow Power Engineering Institute, 105835 Moscow, Russia*

(Dated: November 25, 2018)

Spectral ellipsometry is used to determine the dielectric function of an untwinned crystal of  $\text{LaMnO}_3$  in the range 0.5–5.6 eV at temperatures  $50 \leq T \leq 300$  K. A pronounced redistribution of spectral weight is found at the Néel temperature  $T_N = 140$  K. The anisotropy of the spectral weight transfer matches the magnetic ordering pattern. A superexchange model quantitatively describes spectral weight transfer induced by spin correlations. This analysis implies that the lowest-energy transitions around 2 eV are intersite  $d$ - $d$  transitions, and that  $\text{LaMnO}_3$  is a Mott-Hubbard insulator.

PACS numbers: 75.47.Lx, 78.20.-e, 75.30.-m, 75.30.Et

The physical properties of transition metal oxides with orbital degeneracy are currently a major focus of research. Recent work has shown that the optical spectra of manganites [1, 2], vanadates [3, 4], and ruthenates [5], among others, are highly sensitive to orbital and magnetic ordering phenomena. In an orbitally ordered state, the anisotropy of the optical spectrum reflects the orientation of the valence  $d$ -orbitals with respect to the crystalline axes. Orbital ordering transitions are therefore associated with pronounced rearrangements of the optical spectral weight. It has long been known that magnetic ordering can also induce large shifts of the optical spectral weight of transition metal oxides, but a microscopic understanding of these phenomena has not yet been achieved [6]. This long-standing problem has recently resurfaced in the context of the interplay between spin and orbital degrees of freedom in insulating  $\text{YVO}_3$  and  $\text{LaVO}_3$ , where both magnetic and orbital ordering were found to cause major modifications of the optical spectra [3, 4]. In the vanadates, as well as in other systems with partially occupied  $d$ -orbitals of  $t_{2g}$  symmetry, the spin and orbital dynamics are intimately coupled, so that orbitally and magnetically driven phase transitions occur in the same temperature range. The pertinent ground states, as well as the excited states responsible for the temperature dependent optical conductivity, are currently topics of active debate [7, 8, 9].

In  $\text{LaMnO}_3$ , the insulating parent compound of a family of materials exhibiting “colossal magnetoresistance”, the critical temperatures for orbital ( $T_{OO} = 780$  K) and antiferromagnetic ( $T_N = 140$  K) ordering are very different, and the associated ground states are well understood. A sketch is provided in the inset of Fig. 1.  $\text{LaMnO}_3$  is therefore well suited as a model system to develop a microscopic understanding of the optical spectral weight transfer associated with these phase transitions.

In a prior near-normal-incidence reflectivity study, the anisotropy of the optical spectrum was indeed found to increase markedly below the orbital ordering temperature [1]. However, spectral weight shifts at the Néel temperature were not clearly resolved in the earlier experiments [1, 2], contrary to theoretical predictions [10]. Here we use spectral ellipsometry to accurately monitor the temperature evolution of the dielectric function in the 0.5–5.6 eV range. A marked redistribution of spectral weight is found in the antiferromagnetic state. We also report a detailed, quantitative theoretical description of these data. This provides a solid foundation for the interpretation of the optical spectra of a large class of magnetically ordered transition metal oxides. Our analysis also shows that  $\text{LaMnO}_3$  is a Mott-Hubbard insulator, thus resolving a controversy about the nature of the insulating state.

A  $\text{LaMnO}_3$  crystal was grown by the floating zone method and characterized by energy dispersive X-ray (EDX) analysis, X-ray diffraction, magnetic susceptibility and resistivity measurements [11]. In the as-grown state,  $\text{LaMnO}_3$  single crystals have always heavily twinned domain (or even microdomain) structures. A nearly single-domain sample was obtained by heating above  $T_{OO}$  in air without applying an external stress, and subsequent slow cooling to room temperature. The domain pattern was visualized *in situ* using a high-temperature optical microscope with crossed polarizers and compensator. Using the X-ray Laue technique, we confirmed that the degree of detwinning was better than 85 % over the entire sample surface.

The technique of ellipsometry provides significant advantages over conventional reflection methods in that (i) it is self-normalizing and does not require reference measurements, and (ii)  $\epsilon_1(\nu)$  and  $\epsilon_2(\nu)$  are obtained directly without a Kramers-Kronig transformation. For the ellipsometric measurements the crystal surface was polished to optical grade with diamond powders. The measurements were performed with a home-built ellipsometer of rotating analyzer type [12] where the angle of incidence is  $67.5^\circ$ . The sample was mounted on the cold finger of a helium flow UHV cryostat which is equipped with

\*Also at the Institute of Solid State Physics, Russian Academy of Sciences, Chernogolovka, Moscow distr., 142432 Russia

high-quality stress-free fused-quartz windows. We used a short-arc Xe lamp and a tungsten quartz-iodine lamp, as well as a Si-diode and two photomultipliers to cover the spectral range from 0.5 to 5.6 eV.

Figures 1(a) and 1(b) show representative spectra of the real and imaginary parts of the dielectric function,  $\epsilon_1(\nu)$  and  $\epsilon_2(\nu)$ , along the  $b$ -axis and  $c$ -axis, respectively. The strong anisotropy between  $\epsilon_b$  and  $\epsilon_c$  confirms the substantial detwinning of our crystal. The spectra are dominated by two broad optical bands around 2.0 and 4.8 eV in  $\epsilon_b$ , as compared to 2.5 and 4.5 eV in  $\epsilon_c$ . Superimposed are a number of smaller spectral features. In particular, one can clearly see in room temperature  $\epsilon_b$  spectrum that the low-energy optical band consists of three distinct bands that are reliably resolved thanks to the accuracy of the ellipsometric data. The anisotropy between  $\epsilon_b$  and  $\epsilon_c$  increases with decreasing temperature and becomes most pronounced below  $T_N = 140$  K.

Figure 2 displays the evolution of the optical conductivity,  $\sigma_1(\nu) = 1/(4\pi) \nu \cdot \epsilon_2(\nu)$ , in successive temperature intervals of identical width  $\Delta T = 75$  K. Remarkably, the low-energy bands in  $b$ - and  $c$ -axis polarization exhibit opposite trends. Upon cooling, a drastic *gain* of spectral weight,  $SW = \int \sigma_1(\nu') d\nu'$ , of the  $b$ -axis band at 2.0 eV contrasts with an apparent *SW loss* of the  $c$ -axis band at 2.5 eV. Figure 2 also shows that the total SW along each of the axes is approximately conserved within the investigated spectral range. For  $b$ -axis polarization, SW is transferred from a wide spectral range around 3.7 eV towards the low-energy band centered at 2.0 eV, while for  $c$ -axis polarization, the *loss* of SW around 2.5 eV is compensated by a *SW gain* in the narrow high-energy band centered at 4.4 eV. For both geometries, the shape of the optical conductivity difference spectra,  $\Delta\sigma_1(\nu)$ , is similar in the paramagnetic and antiferromagnetic states. However, the gradual evolution of the SW in the paramagnetic state is strongly enhanced below  $T_N$ . This highlights the influence of spin correlations on the SW shifts.

Figure 3 summarizes the result of a quantitative analysis of the SW changes based on a dispersion analysis of the complex dielectric function. Using a dielectric function of the form  $\epsilon(\nu) = \epsilon_\infty + \sum_j \frac{S_j}{\nu_j^2 - \nu^2 - i\nu\gamma_j}$ , we fit a set of Lorentzian oscillators simultaneously to  $\epsilon_1(\nu)$  and  $\epsilon_2(\nu)$ . In our analysis we assume that the SW of the optical transitions above the investigated energy range remains  $T$ -independent, and for the sake of definiteness we introduce only one high-energy optical band at 8.7 eV with the parameters that have been estimated from the reflectivity data of Arima *et al.* [13, 14]. The dispersion analysis allows us to separate the contributions from the different optical bands in a Kramers-Kronig-consistent way. In particular, a fine structure of the low-energy optical band involving three subbands is reliably resolved. At room temperature, the three low-energy optical bands are centered at 1.9, 2.3, and 2.7 eV in  $\epsilon_b$ , and at 2.1, 2.4, and 2.7 eV in  $\epsilon_c$ . The  $T$ -dependences of  $\nu_j$ ,  $\gamma_j$ , and  $S_j$  of all constituent bands will be given elsewhere [15].

Here we are mainly concerned with the temperature

and polarization dependencies of the relevant low-energy bands, which are presented in Fig. 3 in terms of the effective number of electrons,  $N_{eff} = \frac{2m}{\pi e^2 N} SW$ , where  $m$  is the free electron mass and  $N = a_0^{-3} = 1.7 \times 10^{22} \text{ cm}^{-3}$  is the density of Mn atoms. Fig. 3(a) gives the evolution of the total SW of these low-energy bands, and their separate contributions are detailed in Figs. 3(b) and 3(c). For both polarizations, the two subbands at lower energy (labelled 1 and 2) exhibit the strongest  $T$ -dependence, with noticeable anomalies around  $T_N$ . The weaker band at higher energy (labelled 3) is less  $T$ -dependent.

Figures 1-3 clearly demonstrate that the optical spectral weight in the energy window covered by our experiment is strongly influenced by the onset of antiferromagnetic long-range order, in qualitative agreement with theoretical expectations [10]. Since charge-transfer excitations between manganese  $3d$ -states and oxygen  $2p$ -states are not expected to be affected by the relative orientation of neighboring Mn spins [1], we assign the strongly  $T$ -dependent bands to intersite transitions of the form  $d_i^4 d_j^4 \Rightarrow d_i^3 d_j^5$ . In the ground state below  $T_{OO}$ , one  $e_g$ -orbital of the form  $|\pm\rangle = \cos\frac{\theta}{2}|3z^2 - r^2\rangle \pm \sin\frac{\theta}{2}|x^2 - y^2\rangle$  is occupied by one electron on each Mn site. The two-sublattice orbital ordering pattern is sketched in the inset of Fig. 1. The ‘‘orbital angle’’  $\theta \approx 108^\circ$  is expected from structural data [16]. In the final state, one has to distinguish whether the electron is transferred to an unoccupied or to a half-occupied  $e_g$ -orbital on the neighboring site. The Pauli principle restricts the latter configurations to low-spin (LS) states, while both LS and high-spin (HS) states are allowed in the former case. A detailed analysis along the lines of Refs. [17, 18] yields the following five possible final-state configurations: (i) a HS state of  ${}^6A_1$  symmetry at the energy  $U^* - 3J_H + \Delta_{JT}$ , (ii) a  ${}^4A_1$  LS state at  $U^* + 2J_H + \Delta_{JT}$ , (iii) a  ${}^4E_g$  LS state at  $U^* + 4J_H + \Delta_{JT} - \sqrt{\Delta_{JT}^2 + (4J_H/3)^2}$ , (iv) a  ${}^4E_g$  LS state at  $U^* + 8/3J_H + \Delta_{JT}$ , and (v) a  ${}^4A_2$  LS state at  $U^* + 4J_H + \Delta_{JT} + \sqrt{\Delta_{JT}^2 + (4J_H/3)^2}$ . Here  $U^* = U - V$ ,  $U$  is the Coulomb repulsion on the same  $e_g$ -orbital,  $J_H$  is the Hund interaction, and the parameter  $V$  accounts for the nearest-neighbor excitonic attraction.  $\Delta_{JT}$  is the Jahn-Teller splitting of the  $e_g$ -levels. At  $\Delta_{JT} = 0$  limit, the above level structure coincides with that of Refs. [17, 18]. The magnetic order is of  $A$ -type (inset of Fig. 1), that is, the spin alignment is ferromagnetic in the  $ab$ -plane and antiferromagnetic along the  $c$ -axis. Compared to the paramagnetic state, this favors HS transitions in the  $ab$ -plane and disfavors them along  $c$ , in agreement with the observed SW evolution of the low-energy band at 2 eV (see Fig. 3), which we associate with the HS transition of  ${}^6A_1$  symmetry. The three-subband structure of the band will require more elaborate models that take into account the spatially extended nature of the initial and final states. The higher-energy bands, which exhibit the converse SW evolution below  $T_N$ , are then naturally assigned to the LS transitions.

In Fig. 4 we summarize the evolution of the HS and LS

optical bands, as extracted from the dispersion analysis of the dielectric function at 300 K and 50 K. This figure explicitly shows which optical bands are involved in the SW transfer between the HS- and LS-subbands in the investigated energy range. One can clearly see that the LS-subbands appear in the  $\epsilon_2(\nu)$  spectra above 4 eV, and among them we are able to distinguish only three optical bands at  $4.4 \pm 0.1$  eV,  $4.7 \pm 0.1$  eV, and  $5.7 \pm 0.5$  eV. We suggest the assignment of the  $e_g - e_g$  intersite transitions according to: (i)  $\sim 2.0$  eV, (ii) and (iii)  $\sim 4.4$  eV, (iv)  $\sim 4.7$  eV, and (v)  $\sim 5.7$  eV. The estimated parameters  $U^* \sim 2.8$  eV,  $J_H \sim 0.5$  eV, and  $\Delta_{JT} \sim 0.7$  eV yield a good description of the observed spectra. We notice that the Jahn-Teller splitting of the  $e_g$  levels,  $\Delta_{JT}$ , is much smaller than the on-site correlation energy  $U^*$ . In addition to the  $e_g - e_g$  intersite transitions one could expect also intersite transitions from the occupied  $t_{2g}$ -orbitals to unoccupied  $e_g$ -orbitals (not considered above), which are allowed due to the tilting of the  $\text{MnO}_6$  octahedra. We assign the band at 3.8 eV, which is most pronounced in  $\epsilon_{2c}$ , to the intersite  $t_{2g} - e_g$  HS-transitions. In agreement with our experiment, these transitions are observed at energies shifted up by the crystal field splitting  $10Dq \sim 1.5$  eV [19] with respect to the intersite  $e_g - e_g$  HS-transitions. The polarization dependence of the band at 3.8 eV can be naturally explained by the  $C$ -type ordering of the unoccupied  $e_g$ -orbitals.

We now show that one can obtain a quantitative understanding of the absolute spectral weight transfer induced by antiferromagnetic spin correlations based on this assignment. Via the optical sum rule for tight-binding models [10],  $N_{eff}$  can be expressed as  $N_{eff} = (ma_0^2/\hbar^2)K$ , where  $K$  is the kinetic energy associated with virtual charge fluctuations. The contribution of the HS  ${}^6A_1$  excitation to  $K$  can be calculated from a related term in the superexchange energy,  $K = -2\langle H_{SE}({}^6A_1) \rangle$  [8]. For the bond along the  $\gamma (= a, b, c)$  direction,  $H_{SE}({}^6A_1) = -A(\bar{S}_i\bar{S}_j + 6)(1/4 - \tau_i^{(\gamma)}\tau_j^{(\gamma)})$ , with  $A = t^2/5(U^* - 3J_H + \Delta_{JT})$  [18, 20]. Here,  $t$  is the electron transfer amplitude, and the pseudospin  $\tau^{(\gamma)}$  depends on the orbital state. Calculating its expectation value in terms of the orbital angle  $\theta$ , one obtains for  $T \ll T_{OO}$

$$K^{(b)} = (A/2) \langle \bar{S}_i\bar{S}_j + 6 \rangle^{(b)} (3/4 + \sin^2 \theta), \quad (1)$$

$$K^{(c)} = (A/2) \langle \bar{S}_i\bar{S}_j + 6 \rangle^{(c)} \sin^2 \theta. \quad (2)$$

For  $T \ll T_N$ ,  $\langle \bar{S}_i\bar{S}_j \rangle^{(b)} \rightarrow 4$  and  $\langle \bar{S}_i\bar{S}_j \rangle^{(c)} \rightarrow -4$  within the classical approximation [21], while  $\langle \bar{S}_i\bar{S}_j \rangle^{(b,c)} \rightarrow 0$  for  $T \gg T_N$ . Using  $\theta = 108^\circ$  [16], and taking the value  $t = 0.4$  eV extracted from an analysis of the magnetic data and spin wave dispersions [18, 20], we obtain  $K^{(b)} = 0.14$  eV and  $N_{eff}^{(b)} = 0.28$  for the HS-band at  $T = 0$ . The theoretical low- and high- $T$  limits for different polarizations, indicated in Fig. 3(a) by dashed lines, show a remarkable correspondence with the experimental data. Having the  $t$ -value and  $d_i-d_j$  transition energies obtained above, we can in fact calculate spin exchange constants. Using the superexchange Hamiltonian of Ref. 17, we obtain  $J_c = 1.0$  meV,  $J_{ab} = -1.2$  meV, consistent with magnon data [22, 23].

In summary, the experimentally determined redistribution of the optical SW in  $\text{LaMnO}_3$  is in excellent agreement with a model that attributes these shifts to temperature dependent correlations between Mn spins. This strongly supports our assignment of the lowest-energy band around 2 eV to intersite  $d_i-d_j$  transitions. Figure 4 also shows a strong, weakly temperature dependent contribution to the spectral weight at higher energies around 4.7 eV, which can be attributed to  $O(2p)$ - $\text{Mn}(3d)$  charge-transfer excitations mixed with the higher-energy  $d_i-d_j$  transitions discussed above. Indeed, a ligand-field model for  $\text{MnO}_6$  octahedra predicts a strong  $p-d$  transition at 4.7 eV [19]. This sequence of interband transition energies implies that  $\text{LaMnO}_3$  is a Mott-Hubbard insulator whose insulating nature is determined primarily by strong electronic correlations [24]. We expect that the link between the anisotropic optical spectral weight and the spin-spin correlation function  $\langle \bar{S}_i\bar{S}_j \rangle$  we have uncovered for  $\text{LaMnO}_3$  will provide insights into the optical spectra of other transition metal oxides as well.

We thank A. M. Stoneham and A. M. Oleś for fruitful discussions, T. Holden for the support during ellipsometry measurements, and J. Stremper, C. Ulrich and I. Zegkinoglou for the characterization of the crystal.

- 
- [1] K. Tobe *et al.*, Phys. Rev. B **64**, 184421 (2001).  
[2] M.A. Quijada *et al.*, Phys. Rev. B **64**, 224426 (2001).  
[3] S. Miyasaka, Y. Okimoto, and Y. Tokura, J. Phys. Soc. Jpn. **71**, 2086 (2002).  
[4] A.A. Tsvetkov *et al.*, Phys. Rev. B **69**, 075110 (2004).  
[5] J.S. Lee *et al.*, Phys. Rev. Lett. **89**, 257402 (2002).  
[6] L. Nosenzo, G. Samoggia, and I. Pollini, Phys. Rev. B **29**, 3607 (1984), and references therein.  
[7] C. Ulrich *et al.*, Phys. Rev. Lett. **91**, 257202 (2003).  
[8] G. Khaliullin, P. Horsch, and A.M. Oleś, cond-mat/0403459.  
[9] Y. Motome *et al.*, Phys. Rev. Lett. **90**, 146602 (2003).  
[10] K.H. Ahn and A.J. Millis, Phys. Rev. B **61**, 13545 (2000).  
[11] A.M. Balbashov *et al.*, J. Cryst. Growth **167**, 365 (1996).  
[12] L. Viña, S. Logothetidis, and M. Cardona, Phys. Rev. B **30**, 1979 (1984).  
[13] T. Arima and Y. Tokura, J. Phys. Soc. Jpn. **64**, 2488 (1995); T. Arima and Y. Tokura, J.B. Torrance, Phys. Rev. B **48**, 17006 (1993).  
[14] Y. Okimoto *et al.*, Phys. Rev. B **55**, 4206 (1997).  
[15] N.N. Kovaleva, unpublished.  
[16] J. Rodríguez-Carvajal *et al.*, Phys. Rev. B **57**, R3189

- (1998).
- [17] J.S. Griffith, *The Theory of Transition-Metal Ions* (Cambridge University Press, 1961).
- [18] L.F. Feiner and A.M. Oleś, Phys. Rev. B **59**, 3295 (1999).
- [19] A.S. Moskvin, Phys. Rev. B **65**, 205113 (2002).
- [20] G. Khaliullin and R. Kilian, Phys. Rev. B **61**, 3494 (2000).
- [21] The quantum corrections are small because of large spin and three dimensionality.
- [22] K. Hirota *et al.*, J. Phys. Soc. Jpn. **65**, 3736 (1996):  $J_c = 1.21 \pm 0.05$  meV,  $J_{ab} = -1.67 \pm 0.02$  meV; F. Moussa *et al.*, Phys. Rev. B **54**, 15149 (1996):  $J_c = 1.16$  meV,  $J_{ab} = -1.66$  meV.
- [23] A better fit of *both magnetic and optical data* is in fact achieved at  $\theta = 102^\circ$ :  $J_c = 1.2$  meV,  $J_{ab} = -1.6$  meV, indicating that the orbital angle is slightly reduced from the structural one by superexchange correlations.
- [24] J. Zaanen, G.A. Sawatzky, and J.W. Allen, Phys. Rev. Lett. **55**, 418 (1985).

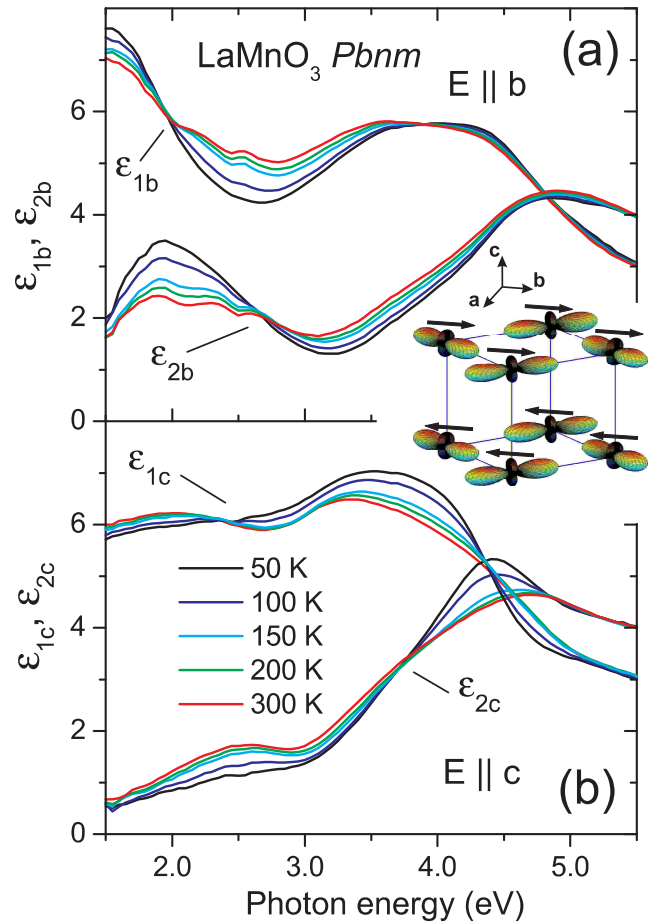


FIG. 1: Temperature variation of dielectric function of a detwinned  $\text{LaMnO}_3$  crystal in (a)  $b$ -axis and (b)  $c$ -axis polarization. Inset. Sketch of  $e_g$  orbital ordering and spin ordering.

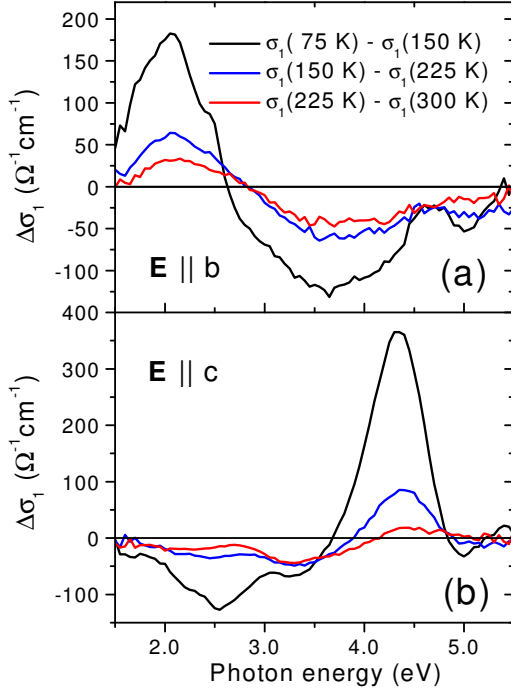


FIG. 2: Difference optical conductivity spectra  $\Delta\sigma_1(\nu)$  for successive temperature intervals of fixed width  $\Delta T = 75$  K in (a)  $b$ -axis and (b)  $c$ -axis polarization. The differences between spectra at 225 and 300 K, and between 150 and 225 K, indicate changes in the paramagnetic state. The difference between spectra at 75 K ( $< T_N$ ) and 150 K ( $> T_N$ ) is due to the onset of antiferromagnetic long-range order.

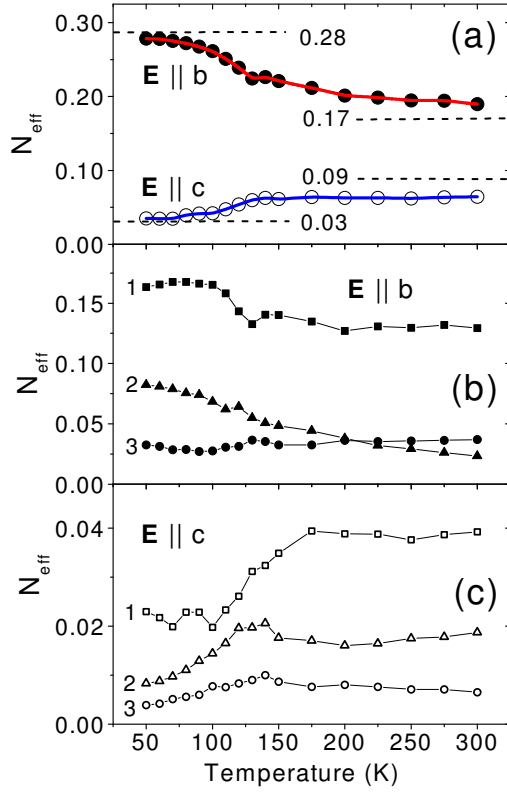


FIG. 3: (a) Temperature and polarization dependence of the total spectral weight  $N_{\text{eff}}$  of the lowest-energy optical band extracted from the dispersion analysis. The dashed lines indicate the low-temperature and asymptotic high-temperature limits estimated from the superexchange model described in the text. The lower panels show the contributions of the three Lorentzian subbands for (b)  $b$ -axis and (c)  $c$ -axis polarization.

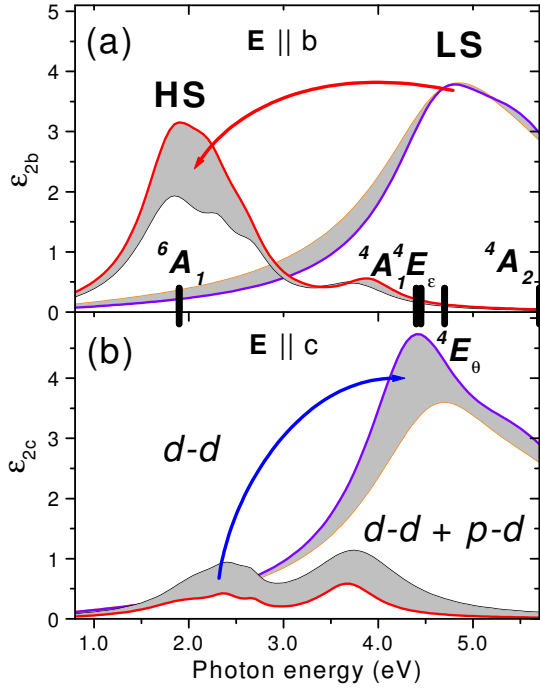


FIG. 4: Summary of the evolution of the HS- and LS-optical bands, as extracted from the dispersion analysis of the dielectric function at 300 K (thin line) and 50 K (thick line) for (a) b-axis and (b) c-axis polarization. The difference is displayed by the shaded area, and the arrows indicate the spectral weight transfer upon cooling. The assignment of the  $d_i - d_j$  transitions is also shown.